Hot exciton cooling and multiple exciton generation in PbSe quantum dots

Kumar, Manoj; Vezzoli, Stefano; Wang, Zilong; Chaudhary, Varun; Ramanujan, Raju Vijayaraghavan; Gurzadyan, Gagik G.; Bruno, Annalisa; Soci, Cesare

2016

Kumar, M., Vezzoli, S., Wang, Z., Chaudhary, V., Ramanujan, R. V., Gurzadyan, G. G., et al. (2016). Hot exciton cooling and multiple exciton generation in PbSe quantum dots. Phys. Chem. Chem. Phys., 18, 31107-31114.

https://hdl.handle.net/10356/85785

https://doi.org/10.1039/C6CP03790A

PCCP

ARTICLE

Hot exciton cooling and multiple exciton generation in PbSe quantum dots

Received 00th January 20xx,
Accepted 00th January 20xx

DOI: 10.1039/x0xx00000x

www.rsc.org/

Manoj Kumar,[a] Stefano Vezzoli,[b] Zilong Wang,[a] Varun Chaudhary,[c, d] Raju V Ramanujan,[d] Gagik G Gurzadyan,[a,e] Annalisa Bruno,*[f] and Cesare Soci,*[a,b]

Multiple exciton generation (MEG) is a promising process to improve the power conversion efficiency of solar cells. PbSe quantum dots (QDs) have shown reasonably high MEG quantum yield (QY) although the photon energy threshold for this process is still under debate. One of the reasons for this inconsistency is the complicated competition of MEG and hot exciton cooling, especially at higher excited states. Here we investigate MEG QY and the origin of the photon energy threshold for MEG in PbSe QDs of three different sizes by studying the transient absorption (TA) spectra, both at the band gap (near infrared, NIR) and far from the band gap energy (visible range). The comparison of visible TA spectra and dynamics for different pump wavelengths, below, around and above MEG threshold, provides evidence of the role of the Σ transition in slowing down the exciton cooling process that can help MEG to take over the phonon relaxation process. The universality of this behavior is confirmed by studying QDs of three different sizes. Moreover our results suggest that MEG QY can be determined by pump-probe experiments probed above the band gap.

1. Introduction

The power conversion efficiency of a single semiconductor junction solar cell (SC) can be, theoretically, as high as 33%.[1] At the moment in a conventional SC, most of the absorbed energy is dissipated in heat. Indeed, in a semiconductor, when the energy (hν) of an absorbed photon is higher than the energy band gap (Eg), hot carriers are generated. Hot carriers quickly cool down to the band edge and release their excess energy to phonons (thermal dissipation). In bulk semiconductors the distribution of energy levels is continuous, so the coupling with phonons is very efficient and consequently the excess energy of hot carriers is quickly dissipated.[2] The process of hot carriers cooling down is then a major energy loss channel in photovoltaic devices.[2, 3] In contrast, in quantum confined nanostructures, the energy levels are discrete, and the energy difference between two consequent energy levels can be much higher than the phonon energy. Therefore, when the energy of the absorbed photon is at least twice the energy band gap, a significant portion of the excess energy of hot excitons can be transferred to electrons/holes in the valence band, hot exciton cooling process through phonon is reduced[4, 5], and one or more new excitons can be created. This process is known as multiple excitons generation (MEG)[6-15] and, in principle, it allows to highly improve the SC power conversion efficiency.[6, 16-18]

Typical MEG quantum yield (QY) values in quantum dots (QDs) are between 1 and 3 with photon energy excitation from 2 to 5 times the band gap of the QDs.[2, 19-22] However there is still an on-going debate about the parameters influencing the MEG QY,[23] since other works have shown very low MEG QY even for much higher photon energy.[24-27] One of the reasons for this inconsistency may be the complicated competition of MEG and hot exciton de-excitation process, especially at higher excited states. In particular, one of the open questions is how the threshold energy for MEG is influenced by other physical phenomena. In principle, the threshold should be two times Eg, but it turns out to be higher since phonon relaxation rates are normally larger than MEG rate. Recently it has been pointed out that the electronic transition, corresponding to the Σ point in the Brillouin zone[i28] called the Σ transition, could play an important role in determining the threshold for MEG.[4] It has been suggested that the hot exciton cooling process could slow down around this level, allowing the MEG process to overcome the cooling rate of phonon.[4] This would imply that MEG has an energy threshold strictly higher than the Σ

[a] Division of Physics and Applied Physics, School of Physical and Mathematical Sciences, Nanyang Technological University, 21 Nanyang Link, Singapore, Singapore, 637371
[b] Centre for Disruptive Photonic Technologies, School of Physical and Mathematical Sciences, Nanyang Technological University, 21 Nanyang Link, Singapore, Singapore, 637371
[c] Interdisciplinary Graduate School (IGS), Nanyang Technological University, 50 Nanyang Avenue, Singapore, Singapore, 639798
[d] School of Materials Science and Engineering, Nanyang Technological University, 50 Nanyang Avenue, Singapore 639798
[e] Institute of Artificial Photosynthesis, State Key Laboratory of Fine Chemical, Dalian University of Technology, Dalian, 116024, China
[f] Energy Research Institute @ NTU (ERI@N), Research Techno Plaza, X-Frontier Block, 50 Nanyang Drive, Singapore, Singapore, 637553

Electronic Supplementary Information (ESI) available. See DOI: 10.1039/x0xx00000x

transition.[4, 8, 10, 29] The Σ transition is observed in both bulk and QDs and its position shifts towards higher energy with decreasing the size of QDs.[28]

PbSe QDs are widely explored as material for SC, infrared (IR) lasers, diodes, and IR-detectors applications. PbSe QDs, due to their large Bohr radius (46 nm), show large quantum confinement effects[30] exhibiting narrow emission ranging from near infrared (NIR) to the mid infrared (IR).[31] Most of the previous spectroscopic studies on PbSe QDs have been performed near the band edge,[2, 8, 32-36] which is at the bottom of the cooling cascade process through the higher energy states, where 1P-1S transition is the last step of the cooling cascade and thus, clear information of the higher energy levels cannot be extracted from the rise time of the photobleaching signal. Therefore, in these studies only cooling process from 1P to 1S, is assessed by probing states in the NIR, close to the QD band gap. The competition between hot exciton cooling and MEG cannot be observed and quantified in the band edge measurements.

In this paper, we determine MEG threshold energy and MEG QY for PbSe QDs of three different sizes through NIR transient absorption (TA) spectra. We also investigated the origin of the threshold energy for MEG in PbSe QDs through the analysis of TA spectra, in the visible region close to the Σ transition, at different pumping energies. We show evidence of a reduction of the hot exciton cooling down via phonon relaxation around the Σ point, where the MEG starts taking over the phonon relaxation process. Moreover by comparing the TA dynamics at and above the PbSe QDs band gap, we also infer that the MEG QY could be measured directly from the visible TA spectra (above the band gap), which is generally easier to measure comparing to the NIR TA spectra.

2. Methodology

2.1 Materials, sample preparation and characterization

Three different types of PbSe QDs having absorption peak at 1100 nm (QD_1), 1200 nm (QD_2) and 1300 nm (QD_3) respectively have been bought from NN Crystal US Corporation suspended in hexane with an initial concentration of 10 mg/ml. They were diluted around 10 times to avoid that most of pumping photons would be absorbed by the front surface of the sample and then filled in quartz cuvettes of 1 mm optical path length for all the optical measurements.

Absorption spectra of PbSe QDs were measured by Perkin Elmer Lambda 750 UV/Vis/NIR spectrophotometer with 1 nm wavelength resolution. Photoluminescence (PL) spectra were measured using a FluoroLog-3 spectrophotometer with wavelength resolution of 0.5 nm using the nitrogen cooled InGaAs detector (Electro-Optical Systems). All measurements were performed at room temperature.

Particle size and morphology of PbSe QDs were determined by using JEOL JEM-2010/UHR transmission electron microscope (TEM) at operating voltage of 200 KV. The hexane suspended PbSe QDs were dropped on a holey carbon-coated copper grid and let dry in vacuum for one night before being measured. QDs averaged sizes were determined from TEM images using the Image J software. From the images individual particles sizes were extrapolated and a histogram distribution was generated. The average QD's size was then calculated by Gaussian fitting of the histograms.

2.4 Transient absorption (TA) measurement

TA setup schemes for Visible and NIR measurements are shown in Figures S1 (a) and Figure S1 (b) in Supporting Information (SI). In both configurations, the fundamental (800 nm) light beam of a Ti:Sapphire femtosecond laser (repetition rate 1KHz, pulse length around 100 fs and 2W power), the second (SH, 400 nm) and the third harmonic (TH, 267 nm) were used as pump beams. The SH was generated using a type-1 BBO crystal (phase matching angle 29.2^0) while the TH was formed by the sum frequency generation of 400 nm and 800 nm in a type-2 BBO crystal (phase matching angle 55.5^0). The pump laser power was tuned by a neutral density (ND) filter and kept low throughout the measurements to minimize the nonlinear multiple-photon absorption by QDs.

The white light continuum (WLC_{vis}) used as probe light for visible TA experiments Figure S1 (a), was generated by focusing the 800 nm beam into a 2 mm thick sapphire plate. WLC_{VIS} was focused on the sample and the spectra were measured using CCD camera (Entwicklungsburo Stresing) with detection range from 200 nm to 950 nm. The white light continuum (WLC_{NIR}) probe light for NIR TA measurements was generated by focusing 1620 nm laser light from the optical parametric amplifier (OPA, Palitra-FS Quantronix), into a 4 mm thick yttrium aluminium garnet (YAG) crystal.[37] The residue of 1620 nm from the WLC_{NIR} is filtered by a short-pass mirror (Thorlabs DMSP1500). WLC_{NIR} was focused on the sample and the signal was detected by a NIR photodiode array (PDA) (Entwicklungsburo Stresing) in the range from 950 nm to 1450 nm. The samples were always shaken by a motorized stage during measurements to minimize the photochemical decomposition.

3. Results and discussion

3.1 PbSe QDs

TEM images of PbSe QD_1, QD_2 and QD_3 are shown in Figure 1 (a), (b) and (c) respectively. All QDs have a spherical shape and their average diameters, estimated from the TEM images, are 3.6±0.3 nm, 3.8±0.5 nm and 4.3±0.5 nm for QD_1, QD_2 and QD_3 respectively. QDs sizes distributions are shown in Figure S2 in SI. In Figure 1 (d), (e) and (f) absorption (left axis) and PL (right axis) spectra of QD_1, QD_2 and QD_3 are shown, with first excitonic absorption peaks at ~ 1100 nm, ~ 1200 nm and ~ 1300 nm and PL peaks at ~ 1170 nm, ~ 1260 nm and ~ 1350 nm, respectively. The well-defined first excitonic peaks in the absorption spectra of all QDs samples correspond to the band gap energy (Eg) value. As expected, we consistently observe a red shift in the measured first excitonic absorption as well as

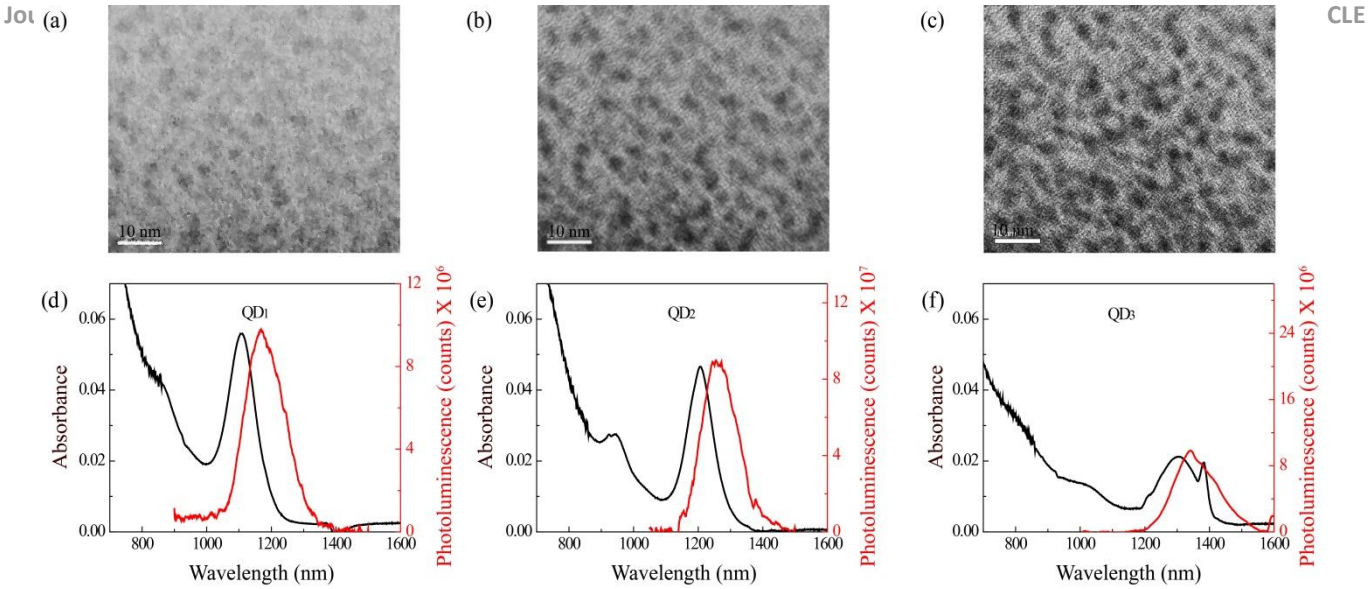

Figure 1. TEM images of (a) QD_1, (b) QD_2 and (c) QD_3. Steady state absorption (left axis) and photoluminescence spectra (right axis), with 800 nm excitation for (d) QD_1, (e) QD_2 and (f) QD_3.

PL peaks coincide well with increasing size of QDs sizes obtained from TEM images.

To identify the optical transitions of the three QDs, the second derivative of their absorption spectra were calculated and reported in Figure 2 for QD_1 and in Figure S3, in SI, for QD_2 and QD_3.[28, 38, 39] The first minima of the second derivative curve in Figure 2, around 600 nm has been unambiguously assigned to the Σ transition,[28, 33] which can be detected by the visible TA measurements as shown and discussed in section 3.3. The assignment of the second dip (~ 870 nm) is still under debate. Hui *et al* assigned, on the base of theoretical calculations using k•p model,[40-42] to the $1S_{he}1P_{eh}$ transition, that is not optically allowed.[ii] Liljeorth *et al* and several others defined this second transition as $1P_{he}1P_{eh}$ based on pump-probe measurements and density of states measured by scanning tunnelling spectroscopy.[43-46] The last minima of the second derivative curve at ~1100 nm which corresponds to the first excitonic

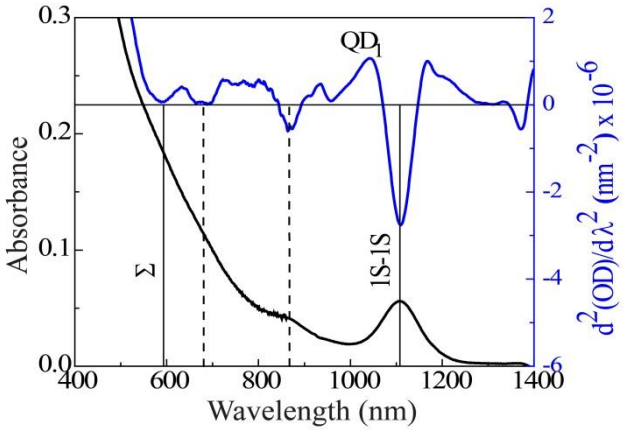

Figure 2. QD_1 absorption spectra (black line) and its second derivative (blue line)

absorption peak, is assigned to the 1S-1S transition.[28]

3.2 Near infrared transient absorption (NIR TA) spectra and MEG QY

Figures 3 (a), (b) and (c) show the NIR TA spectra of QD_1 at pump wavelengths of 800 nm (corresponding to 1.38Eg), 400 nm (2.75Eg) and 267 nm (4.14Eg). Results for QD_2 and QD_3 can be found in Figure S4 and S5 in SI, respectively. For all the pump wavelengths the laser fluence was kept low enough to reduce the multiphoton absorption by QDs. Pump fluences of 10μJ/cm^2 (4.03X10^{13} photons/pulse-cm^2) for 800 nm and 5μJ/cm^2 (1.01X10^{13} photons/pulse-cm^2 for 400 nm and 0.67X10^{13} photons/pulse-cm^2 for 267 nm) for 400 nm and 267 nm pump wavelengths were used in TA measurements. The average number of photons absorbed per pulse by a QD, N_{abs}, was calculated using the product of the fluence (f) and the absorption cross section (σ) at the pump wavelength (N_{abs} = f•σ).[47] The absorption cross sections were calculated following the method proposed by Giblin et. al.[48] All the details of the method are reported in S.I. N_{abs} values at pump wavelengths of 800 nm, 400 nm and 267 nm are 0.031, 0.042 and 0.172 for QD_1, 0.037, 0.050 and 0.203 for QD_2 and 0.054, 0.072 and 0.294 for QD_3respectively. The fluence dependent kinetics of the QD_1 at 800 nm pump and 1100 nm probe wavelength is reported in Figure S6, in SI, showing that all the measurements were performed in a low fluency regime

The spectra in Figure 3 (a), (b) and (c) display similar features, however time evolution for three pump wavelengths are different. The positive band around 1000 nm is due to the excited state absorption (ESA).[40, 41] The main negative signal dominating the spectra at around 1100 nm corresponds to the ground state photobleaching (GSB). The GSB is due to depletion of the ground state carriers to excited states and it represents the 1S-1S transition as discussed before.[21, 28, 49, 50] In addition to the GSB valley a broad positive band at longer

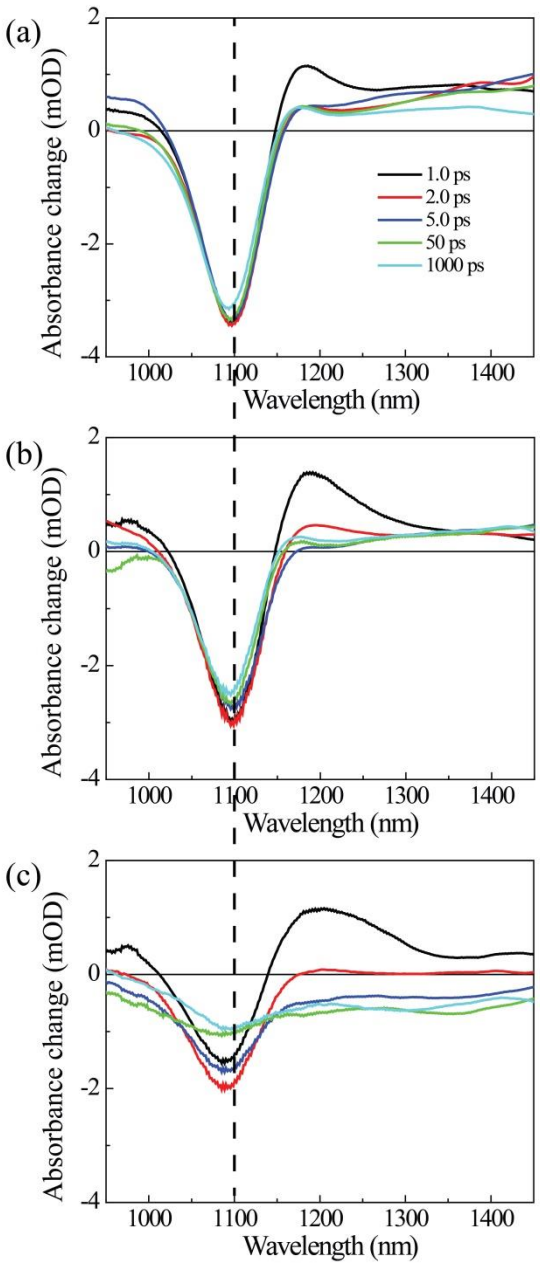

Figure 3. TA spectra of PbSe QD_1 with pump wavelengths of (a) 800 nm, (b) 400 nm and (c) 267 nm

wavelengths due to the Coulomb interaction between the excitons is observed.[21]

In Figure 4, the GSB dynamics of QD_1 for different pump wavelengths are shown after normalization with their long time tail. After excitation with 800 nm (1.38 Eg, black circle), the kinetics presents a fast rise (<0.5 ps), a small and fast decaying differential signal in first few ps due to a small amount of multi-photon absorption followed by a very long decay, much longer than our time scale of 1 ns. The long decay has been attributed to single exciton radiative recombination, which is of the order of microseconds in PbSe QDs.[26, 32] The kinetics with 400 nm pump (2.75Eg, blue squares) shows the fast rise and then fast decay in first tens of ps and followed by long decay. The fast decay could be due to the Auger

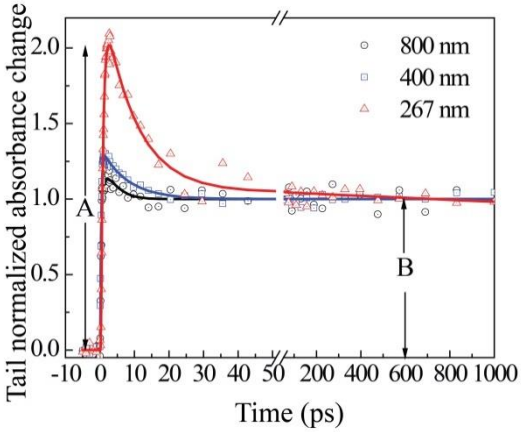

Figure 4. QD_1 tail normalized TA kinetics with pump wavelengths of 800 (black circle), 400 (blue square) and 267 nm (red triangle) and probe wavelength of 1100 nm. Symbols are data points and solid lines are bi- exponential fits.

recombination of multiple hot excitons in QDs before relaxing into the long lived single exciton state.[26] For 267 nm excitation (4.14Eg, red triangles), we observe a slow rise around 1 ps, and a fast decay in the first 50 ps followed by long decay. The slow rise time can be explained as the cool down process of hot excitons towards the band edge and the fast decay is due to a more efficient Auger recombination of multiple excitons with higher energy excitation. It is also reflected as a blue shift of GSB signal (~ 10 nm at 1 ps delay) in Figure 3(c).[21] The observation of Auger recombination of hot excitons and their lifetimes in PbSe QDs coincide well with previous literature results.[26, 32]

From these decays it is possible to evaluate the MEG process and its quantum yield. MEG QY is defined as the number of excitons generated per photon absorbed. Experimentally, MEG QY can be calculated as A/B from the dynamics of excitons GSB signal at the bandgap.[2, 51] Indeed, assuming A being the maximum amplitude value of the dynamics, which is around 1 ps in our cases, and B being the amplitude of dynamics at long delay time, as shown in Figure 4, MEG QY can be calculated as A/B for all the dynamics:[2, 51]

$$\text{MEG QY} = A/B \quad (1)$$

Direct generation of multiple excitons via absorption of multiple photons can be misled to measure MEG QY.[52, 53] For accuracy of MEG estimation, we have taken into account the influence of the direct generation of multiple excitons via absorption of multiple photons introducing a correction factor in equation 1, based on Poisson distribution of photon absorption [$p = (1 - \exp(-N_{abs}))/N_{abs}$].[21] Accurate MEG QY can be calculated using the following equation:

$$\text{MEG QY} = p(A/B) \quad (2)$$

In our measurements we have evaluated MEG QY=1.11 close to the theoretical MEG QY=1 value for 800 nm (1.38Eg) excitation. At 400 nm (2.75Eg) excitation MEG QY was 1.25, which implies the multiple excitons were likely generated by one photon since the excitation photon energy is more than

two times of the bandgap energy (2.75Eg). On the other hand MEG QY=1.84, meaning that approximately two excitons were generated per absorbed photon with 267 nm (4.14Eg) excitation. MEG QY of QD_2 and QD_3 were also determined at the same excitation wavelength and the corresponding TA dynamics are shown in Figure S7(a) and S7(b) respectively.

Table 1 summarizes the calculated MEG QY for QD_1, QD_2 and QD_3. MEG QY varies for different sizes of QDs as a function of excitation photon energy and the bandgap energy ratio ($h\nu/Eg$). MEG QY versus $h\nu/Eg$ is shown in SI Figure S8. From a linear fit, the extracted MEG QY at 4Eg for QD_1, QD_2 and QD_3 are 1.82, 1.77 and 1.70 respectively.[54] Here, we conclude that photon energy at 400 nm is close to the threshold energy for the MEG process to overcome the phonon relaxation. Our results are consistent with the threshold values of 2.5Eg - 3.0Eg reported for similar sizes PbSe QDs.[35, 55]

Table 1. Pump wavelengths, corresponding $h\nu/Eg$ values and MEG QY for QD_1, QD_2 and QD_3

Pump Wavelength (nm)	QD_1		QD_2		QD_3	
	$h\nu$ / Eg	MEG QY	$h\nu$ / Eg	MEG QY	$h\nu$ / Eg	MEG QY
800	1.38	1.11	1.50	1.13	1.63	1.13
400	2.75	1.25	3.00	1.28	3.25	1.33
267	4.12	1.84	4.49	2.07	4.87	2.17

3.3 Visible transient absorption (TA) spectra

Visible TA spectra of PbSe QD_1, QD_2 and QD_3 in the range from 480 nm to 720 nm were measured for different pump wavelengths, below (800 nm), above (267 nm) and close (400 nm) to the MEG threshold and are presented in the SI Figures S8, S9 and S10 in the time interval from 0 to 1000 ps.

TA spectra at 5 and 100 ps pump-probe delays at 800 nm excitation (where no MEG process occurs) are shown in Figure 5 (a), (b) and (c) for QD_1, QD_2 and QD_3 respectively together with their absorption spectra first derivative. TA spectra show a photo-induced absorption signal (positive) over all the visible range. In a previous work the photo-induced absorption peak in PbSe QDs has been attributed due to the Coulomb interaction between the excitons generated by the pump and the excitons generated by the probe pulse.[56] In the same paper they have shown that TA spectra divided by the first derivative of the linear absorption spectrum are proportional to the intensity of the Coulomb interaction energy, *J*. Moreover the authors found that the Coulomb interaction is nearly wavelength independent above 550 nm and that the transient signal close to the band edge photo-bleaching signal has a rise time followed by a slow dynamics, corresponding to the band-edge exciton radiative lifetime. The first implies that Coulomb interaction *J* is independent of the energy level of the probe exciton. The second implies that the Coulomb interaction of the newly created exciton hot pump exciton with the hot probe exciton, J_{HH}, is much smaller than the interaction after the thermal relaxation of the hot pump

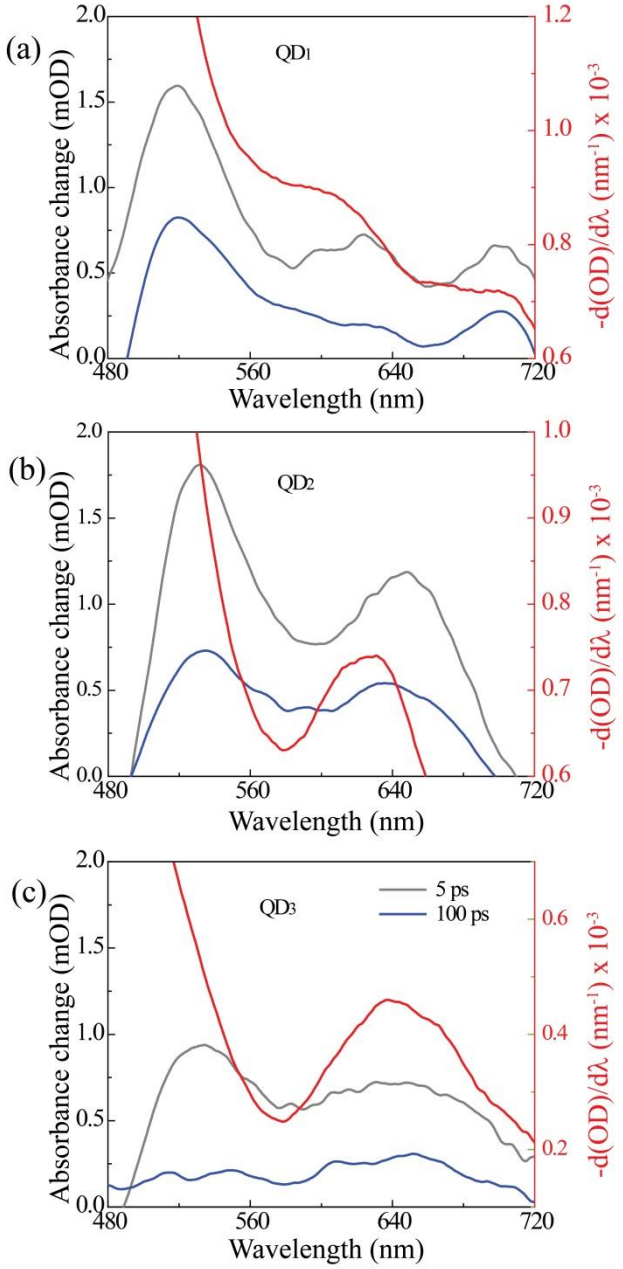

Figure 5. TA spectra at 5 ps (gray line) and 100 ps (blue line) delays with first derivative of absorption spectra (red line) of (a) QD_1, (b) QD_2 and (c) QD_3 using 800 nm pump wavelength

exciton to the band edge (cold) J_{HC}, $|J_{HH}| << |J_{HC}|$. Our data above 550 nm well reproduce the previous observations. In addition, we also present data in the spectral range smaller than 550 nm showing that *J* fast decreases below 530 nm and vanishes for 480 nm, implying that Coulomb interaction is not effective at highly excited energy levels. A fast dynamics for the peak centred~ 525 nm is due to a thermalization process within the fine energy levels far from the band edge. The thermalization does not affect the photo-bleaching of 1100 nm probe (black circles in Figure 4) because the population of the

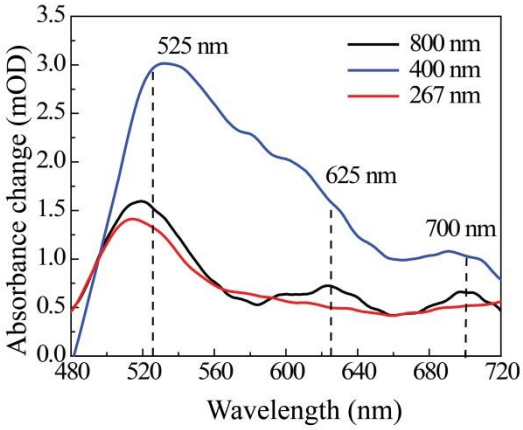

Figure 6. TA spectra (at 5 ps delay) of QD_1 using pump wavelengths of 800 nm (below MEG threshold energy, black line), 400 nm (close to MEG threshold energy, blue line) and 267 nm (above MEG threshold energy, red line)

band edge energy level does not change, but it can affect the Coulomb interaction with higher energy states.

In order to study the single exciton relaxation below, close and above the MEG threshold energy, we analyse the TA spectra (Figure 6) and dynamics (Figure 7 (a), (b) and (c)) with pump energies of 800 nm, 400 nm and 267 nm for QD_1. We focus our discussion here on QD_1 since we found similar trends for all QDs. Both spectra and TA dynamics for QD_1, QD_2 and QD_3 are provided in the SI (Figure S9 to S13). In Figure 6, TA spectra of QD_1 at 5 ps delay for the three pump energies are reported, the spectra are qualitatively similar at all delay times. TA spectra at three pump wavelengths show peaks at 525 nm, 625 nm and 700 nm. The spectrum with pump wavelength at 400 nm (close to the MEG threshold) exhibits strong and structured photo-induced signal at 625 nm and 525 nm, while the spectra with 800 nm and 267 nm pump are very similar showing a less structured signal. Geiregat et al. studied TA spectra in the visible region in PbS QDs.[4] When they used pump energy above the Σ transition they observed a fast photo-bleaching (a fast negative signal in the first 1-2 ps) for probe energy corresponding to the Σ point. Conversely, when using pump energy below the Σ transition, they did not observed any bleaching. In our measured visible TA spectra of PbSe QDs, we do not observed any bleaching both with pumping energies above and below the Σ transition (Figures S9-S11) maybe due to the weak bleaching signal, and thus it could be hidden by the noise.

Figure 7 shows the normalized dynamics of the *hot excitons,* TA signal generated by 800 nm (a), 400 nm (b) and 267 nm (c) excitations and probed at 525 nm, 625 nm and 700 nm. The TA dynamics were deconvoluted and fitted by a single exponential rise and decay plus a constant for the long decays. In Figure 7(a) where no MEG process occurs, the fast rise/decay times are about 0.2 ps/2 ps for 525 nm, 0.3 ps/3 ps for 625 nm and 0.5 ps/4 ps for 700 nm respectively. After the very fast decay, the curves reach an almost asymptotic value for all wavelengths, as illustrated in the inset of Figure 7 (a).

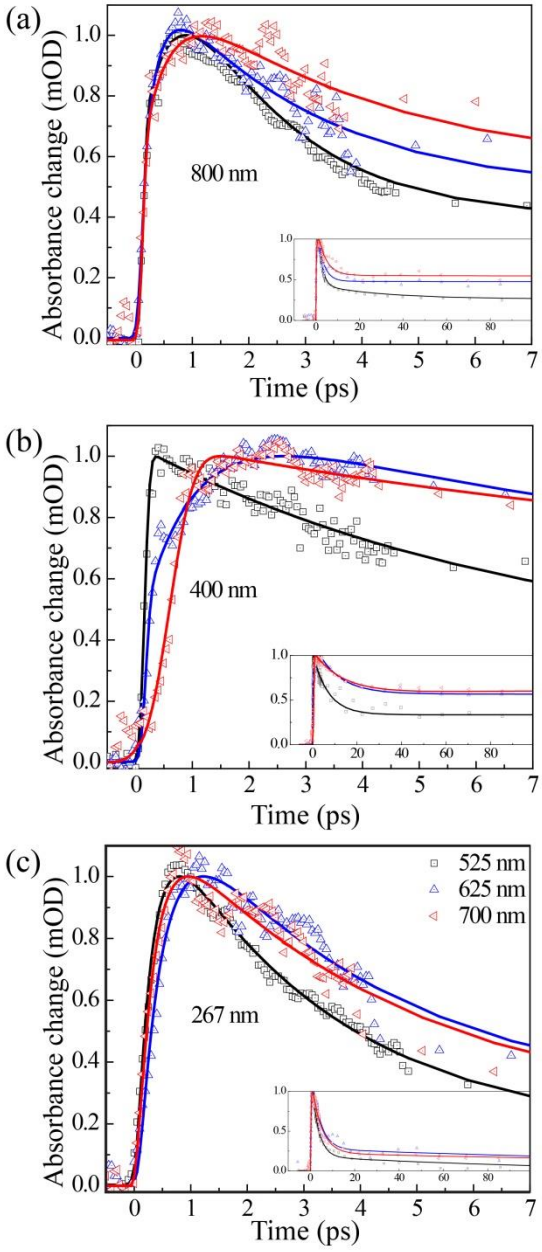

Figure 7. Normalized TA dynamics of QD_1 using pump wavelengths of (a) 800 nm, (b) 400 nm and (c) 267 nm. In each Figure, probe wavelengths are 525 nm (black), 625 nm (blue) and 700 nm (red). Inset of Figures show kinetics for long delays. Symbols are data points and solid lines are bi- exponential fits.

This very long decay time is associated with the radiative recombination of the excitons at the band edge.[56]

The TA dynamics of QD_1 excited at 400 nm are shown in Figure 7 (b); remarkable difference from the decay obtained with 800 nm excitation was observed. Indeed, the rise times at 525 nm are similar with both pump excitations (0.2 ps at 800 nm, 0.1 ps at 400 nm), while the rise times at 625 nm (1ps) and 700 nm (2 ps) are longer for 400 nm pump. Similar behaviour is observed for QD_2 and QD_3 (Figure S12 and S13 in SI). Moreover, TA dynamics present rather long decay times (around 5 ps at 525 nm, 10 ps at 625 nm and 13 ps at 700 nm

probe) as compared to those observed in 800 nm and also to the 267 nm pump case, as will be discussed later. We remind that the Σ transition lays around 600 nm, i.e. in between the 525 nm and the 625 nm peaks, as illustrated in Figure 2 and in Figure S3. Given that the Σ transition is around 600 nm in PbSe QDs, the hot exciton generated by the 400 nm pump thermally relaxes towards the Σ level, thus, the fast rise of photo-induced absorption signal probing at 525 nm can be related to the quick thermal relaxation of hot excitons towards the Σ level. Around the Σ transition, there is a bottleneck for the phonons, which slows down the thermal relaxation of hot exciton. Therefore, the hot exciton dynamics probed above 600 nm (625 nm and 700 nm) present a much slower rise and longer decay time. The long decay after 30 ps reflects the exciton radiative lifetime. There is still an on-going debate regarding the existence of the phonon bottleneck.[57, 58] Some previous studies have attributed the slowing down of charge carrier cooling to the a phonon scattering bottleneck in a critical point of the Brillouin zone[4, 58] while others do support this interpretation since the high energy levels are continue.[57] Prezhdo et. al. suggested the presence of the electron-phonon bottleneck in the semi discrete energy levels just above the bandgap.[57] Our results seem to support the existence of the electron-phonon bottleneck around the Σ transition.

TA dynamics of QD_1 pump by 267 nm beam shows similar trend to that of 800 nm pump (Figure 7(c)) with a slightly longer rise time (about 1 ps) corresponding to the MEG cooling.[19] The fast decay times are around 3.5 ps, 4 ps and 4.5 ps for 525 nm, 625 nm and 700 nm probe wavelengths, respectively. The analogy of 800 nm and 267 nm pump dynamics implies that the hot exciton relaxes following the same process once generated regardless of whether the MEG occurred in QD_1. On the other hand, around the MEG threshold energy (Figure 7(b)), the phonon bottleneck due to the Σ transitions become significant so hot exciton cooling process has to overtake the phonon relaxation channel in order to overcome the MEG threshold. it is clear that when pump energy is well above threshold, MEG dominates over phonon relaxation: the highly energetic exciton generated by the 267 nm pump photon quickly decays to the band edge, by creating additional excitons; the additional excitons recombine non-radiatively via Auger recombination by giving up their energy to the third charge; finally, the last exciton decays radiatively.

Table 2. MEG QY_{525} of PbSe QD_1, QD_2 and QD_3 with 525 nm probe wavelength and 800 nm, 400 nm and 267 nm pump wavelengths

Pump wavelength (nm)	MEG QY_{525}		
	QD_1	QD_2	QD_2
800	1	1	1
400	1.10	1.16	1.09
267	2.19	2.29	2.38

Geiregat et al. calculated the coulomb interaction energy of excitons and found it to be proportional to the number of excitons. So, the amplitude of the TA spectra should also be proportional to the number of generated excitons. In a similar way, we suggest that it is possible to estimate the MEG QY by comparing the dynamics in the visible region following the same definition of MEG QY at bandgap instead of calculating the Coulomb interaction energy of excitons. In other words, the ratio between the values of A/B for the kinetics in the visible with different excitations can be an estimation of the MEG QY. Indeed, the A/B ratio has been measured at 525 nm probe wavelength ($(A/B)_{525}$) and at excitation wavelengths of 800 nm, 400 nm and 267 nm for all the QD_1, QD_2, and QD_3 as shown in Figure S14 and table S1. As discussed before, just after the excitation, hot-hot, hot-cold and cold-cold excitons interactions etc. are taking place. Due to these effects $(A/B)_{525}$ values can be higher than the A/B values. Since there is no MEG with 800 nm excitation, $(A/B)_{525}$ for all three excitation wavelengths are normalized with respect to the $(A/B)_{525}$ value obtained at 800 nm, results are shown in table 2. MEG QY_{525} is comparable to the MEG QY for all three measured QDs as shown in table 1. Therefore, here we demonstrate MEG QY can be measured in the visible region above the band gap of QDs. This observation deserves further investigation.

4. Conclusions

In this work, we study the TA spectra and their dynamics in NIR and visible regions of PbSe QDs of three sizes ranging from 3.6 nm to 4.3 nm. MEG QY were measured at the band gap for different excitation photon energies and the values extrapolated at four times the QD band gap are 1.82, 1.77 and 1.70, for QD_1, QD_2 and QD_3 respectively.

Visible TA spectra were studied around the Σ transition for different pump energies: below, close and above MEG threshold. Our analysis provides a clear evidence of the role of the Σ transition in slowing down the exciton cooling process. The universality of this behaviour is confirmed by the similar behaviour displayed by QDs of different sizes. In conclusion, here we show that TA spectra dynamics in the visible range can provide essential information to interpret the dynamics of MEG and possibly use to assess MEG QY.

Acknowledgements

The authors wish to thank the Singapore Ministry of Education, for financial support through the projects MOE2013-T2-1-044 and MOE2011-T3-1-005.

Notes and references

1 M. C. Hanna and A. J. Nozik, *J. Appl. Phys.*, 2006, **100**, 074510.

2 R. D. Schaller and V. I. Klimov, *Phys. Rev. Lett.*, 2004, **92**, 186601.

3 A. Le Bris and J.-F. Guillemoles, *Appl. Phys. Lett.*, 2010, **97**, 113506.

4 P. Geiregat, C. Delerue, Y. Justo, M. Aerts, F. Spoor, D. Van Thourhout, L. D. A. Siebbeles, G. Allan, A. J. Houtepen and Z. Hens, *ACS Nano*, 2015, **9**, 778.

5 M. C. Beard, A. G. Midgett, M. C. Hanna, J. M. Luther, B. K. Hughes and A. J. Nozik, *Nano Lett.*, 2010, **10**, 3019.

6 O. E. Semonin, J. M. Luther, S. Choi, H.-Y. Chen, J. Gao, A. J. Nozik and M. C. Beard, *Science*, 2011, **334**, 1530.

7 L. A. Padilha, J. T. Stewart, R. L. Sandberg, W. K. Bae, W.-K. Koh, J. M. Pietryga and V. I. Klimov, *Nano Lett.*, 2013, **13**, 1092.

8 A. G. Midgett, J. M. Luther, J. T. Stewart, D. K. Smith, L. A. Padilha, V. I. Klimov, A. J. Nozik and M. C. Beard, *Nano Lett.*, 2013, **13**, 3078.

9 P. D. Cunningham, J. E. Boercker, E. E. Foos, M. P. Lumb, A. R. Smith, J. G. Tischler and J. S. Melinger, *Nano Lett.*, 2011, **11**, 3476.

10 J. J. H. Pijpers, R. Ulbricht, K. J. Tielrooij, A. Osherov, Y. Golan, C. Delerue, G. Allan and M. Bonn, *Nat Phys*, 2009, **5**, 811.

11 Q. Shen, K. Katayama and T. Toyoda, *J. Energy Chem.*, 2015, **24**, 712.

12 J. Gao, A. F. Fidler and V. I. Klimov, *Nat Commun*, 2015, **6**.

13 S. Ten Cate, C. S. S. Sandeep, Y. Liu, M. Law, S. Kinge, A. J. Houtepen, J. M. Schins and L. D. A. Siebbeles, *Acc. Chem. Res.*, 2015, **48**, 174.

14 A. Al-Otaify, S. V. Kershaw, S. Gupta, A. L. Rogach, G. Allan, C. Delerue and D. J. Binks, *Phys. Chem. Chem. Phys.*, 2013, **15**, 16864.

15 A. Sills and M. Califano, *Phys. Chem. Chem. Phys.*, 2015, **17**, 2573.

16 Z. E. R. Abrams, M. Gharghi, A. Niv, C. Gladden and X. Zhang, *Sol. Energy Mater. Sol. Cells*, 2012, **99**, 308.

17 N. J. L. K. Davis, M. L. Bohm, M. Tabachnyk, F. Wisnivesky-Rocca-Rivarola, T. C. Jellicoe, C. Ducati, B. Ehrler and N. C. Greenham, *Nat Commun*, 2015, **6**.

18 M. L. Böhm, T. C. Jellicoe, M. Tabachnyk, N. J. L. K. Davis, F. Wisnivesky-Rocca-Rivarola, C. Ducati, B. Ehrler, A. A. Bakulin and N. C. Greenham, *Nano Lett.*, 2015, **15**, 7987.

19 R. J. Ellingson, M. C. Beard, J. C. Johnson, P. Yu, O. I. Micic, A. J. Nozik, A. Shabaev and A. L. Efros, *Nano Lett.*, 2005, **5**, 865.

20 M. C. Beard, K. P. Knutsen, P. Yu, J. M. Luther, Q. Song, W. K. Metzger, R. J. Ellingson and A. J. Nozik, *Nano Lett.*, 2007, **7**, 2506.

21 J. Sun, W. Yu, A. Usman, T. T. Isimjan, S. Dgobbo, E. Alarousu, K. Takanabe and O. F. Mohammed, *J. Phys. Chem. Lett.*, 2014, **5**, 659.

22 A. a. O. El-Ballouli, E. Alarousu, A. Usman, J. Pan, O. M. Bakr and O. F. Mohammed, *ACS Photonics*, 2014, **1**, 285.

23 D. J. Binks, *Phys. Chem. Chem. Phys.*, 2011, **13**, 12693.

24 I. Gdor, C. Yang, D. Yanover, H. Sachs, E. Lifshitz and S. Ruhman, *J. Phys. Chem. C*, 2013, **117**, 26342.

25 G. Nair, S. M. Geyer, L.-Y. Chang and M. G. Bawendi, *Phys. Rev. B*, 2008, **78**, 125325.

26 J. A. McGuire, M. Sykora, J. Joo, J. M. Pietryga and V. I. Klimov, *Nano Lett.*, 2010, **10**, 2049.

27 S. J. O. Hardman, D. M. Graham, S. K. Stubbs, B. F. Spencer, E. A. Seddon, H.-T. Fung, S. Gardonio, F. Sirotti, M. G. Silly, J. Akhtar, P. O'Brien, D. J. Binks and W. R. Flavell, *Phys. Chem. Chem. Phys.*, 2011, **13**, 20275.

28 R. Koole, G. Allan, C. Delerue, A. Meijerink, D. Vanmaekelbergh and A. J. Houtepen, *Small*, 2008, **4**, 127.

29 G. Nootz, L. A. Padilha, L. Levina, V. Sukhovatkin, S. Webster, L. Brzozowski, E. H. Sargent, D. J. Hagan and E. W. Van Stryland, *Phys. Rev. B*, 2011, **83**, 155302.

30 A. Lipovskii, E. Kolobkova, V. Petrikov, I. Kang, A. Olkhovets, T. Krauss, M. Thomas, J. Silcox, F. Wise, Q. Shen and S. Kycia, *Appl. Phys. Lett.*, 1997, **71**, 3406.

31 J. M. Pietryga, D. J. Werder, D. J. Williams, J. L. Casson, R. D. Schaller, V. I. Klimov and J. A. Hollingsworth, *J. Am. Chem. Soc.*, 2008, **130**, 4879.

32 R. D. Schaller, V. M. Agranovich and V. I. Klimov, *Nat Phys*, 2005, **1**, 189.

33 J. E. Murphy, M. C. Beard, A. G. Norman, S. P. Ahrenkiel, J. C. Johnson, P. Yu, O. I. Mićić, R. J. Ellingson and A. J. Nozik, *J. Am. Chem. Soc.*, 2006, **128**, 3241.

34 J. A. McGuire, J. Joo, J. M. Pietryga, R. D. Schaller and V. I. Klimov, *Acc. Chem. Res.*, 2008, **41**, 1810.

35 C. Smith and D. Binks, *Nanomaterials*, 2013, **4**, 19.

36 T. Nishihara, H. Tahara, M. Okano, M. Ono and Y. Kanemitsu, *J. Phys. Chem. Lett.*, 2015, **6**, 1327.

37 M. Bradler, P. Baum and E. Riedle, *Appl. Phys. B*, 2009, **97**, 561.

38 S. L. Sewall, R. R. Cooney, K. E. H. Anderson, E. A. Dias and P. Kambhampati, *Phys. Rev. B*, 2006, **74**, 235328.

39 L. Cademartiri, E. Montanari, G. Calestani, A. Migliori, A. Guagliardi and G. A. Ozin, *J. Am. Chem. Soc.*, 2006, **128**, 10337.

40 J. J. Peterson, L. Huang, C. Delerue, G. Allan and T. D. Krauss, *Nano Lett.*, 2007, **7**, 3827.

41 J. M. Harbold, H. Du, T. D. Krauss, K.-S. Cho, C. B. Murray and F. W. Wise, *Phys. Rev. B*, 2005, **72**, 195312.

42 H. Du, C. Chen, R. Krishnan, T. D. Krauss, J. M. Harbold, F. W. Wise, M. G. Thomas and J. Silcox, *Nano Lett.*, 2002, **2**, 1321.

43 P. Liljeroth, P. A. Z. van Emmichoven, S. G. Hickey, H. Weller, B. Grandidier, G. Allan and D. Vanmaekelbergh, *Phys. Rev. Lett.*, 2005, **95**, 086801.

44 J. M. Schins, M. T. Trinh, A. J. Houtepen and L. D. A. Siebbeles, *Phys. Rev. B*, 2009, **80**, 035323.

45 M. T. Trinh, A. J. Houtepen, J. M. Schins, J. Piris and L. D. A. Siebbeles, *Nano Lett.*, 2008, **8**, 2112.

46 I. Gdor, H. Sachs, A. Roitblat, D. B. Strasfeld, M. G. Bawendi and S. Ruhman, *ACS Nano*, 2012, **6**, 3269.

47 J. M. Luther, M. C. Beard, Q. Song, M. Law, R. J. Ellingson and A. J. Nozik, *Nano Lett.*, 2007, **7**, 1779.

48 J. Giblin and M. Kuno, *J. Phys. Chem. Lett.*, 2010, **1**, 3340.

49 P. Kambhampati, *J. Phys. Chem. C*, 2011, **115**, 22089.

50 K. Zheng, K. Žídek, M. Abdellah, W. Zhang, P. Chábera, N. Lenngren, A. Yartsev and T. Pullerits, *J. Phys. Chem. C*, 2014, **118**, 18462.

51 M. Ji, S. Park, S. T. Connor, T. Mokari, Y. Cui and K. J. Gaffney, *Nano Lett.*, 2009, **9**, 1217.

52 K. J. Karki, F. Ma, K. Zheng, K. Zidek, A. Mousa, M. A. Abdellah, M. E. Messing, L. R. Wallenberg, A. Yartsev and T. Pullerits, *Sci. Rep.*, 2013, **3**, 2287.

53 N. Lenngren, T. Garting, K. Zheng, M. Abdellah, N. Lascoux, F. Ma, A. Yartsev, K. Žídek and T. Pullerits, *J. Phys. Chem. Lett.*, 2013, **4**, 3330.

54 M. Aerts, T. Bielewicz, C. Klinke, F. C. Grozema, A. J. Houtepen, J. M. Schins and L. D. A. Siebbeles, *Nat Commun*, 2014, **5**.

55 S. ten Cate, Y. Liu, C. S. Suchand Sandeep, S. Kinge, A. J. Houtepen, T. J. Savenije, J. M. Schins, M. Law and L. D. A. Siebbeles, *J. Phys. Chem. Lett.*, 2013, **4**, 1766.
56 P. Geiregat, A. Houtepen, Y. Justo, F. C. Grozema, D. Van Thourhout and Z. Hens, *J. Phys. Chem. C*, 2014, **118**, 22284.
57 O. V. Prezhdo, *Chem. Phys. Lett.*, 2008, **460**, 1.
58 P. Yu, J. M. Nedeljkovic, P. A. Ahrenkiel, R. J. Ellingson and A. J. Nozik, *Nano Lett.*, 2004, **4**, 1089.

[i] Σ point is defined as the second extremum (maxima of the valence band and minima of the conduction band) in the Brillouin zone.

The k•p model is usually used to calculate band structure and optical properties of crystalline materials. In k•p model, the analysis of perturbed term k•p (where k is wave vector and p is momentum operator vector) of the Hamiltonian provide the information of the energy levels and the wave function of the energy levels. The k•p model is usually used to calculate band structure and optical properties of crystalline materials